Simulations of the emission spectra of fac-tris(2-phenylpyridine) iridium and Duschinsky rotation effects using the Herman–Kluk semiclassical initial value representation method

Yinghua Wu and Jean-Luc Brédas

Citation: J. Chem. Phys. **129**, 214305 (2008); doi: 10.1063/1.3027514
View online: http://dx.doi.org/10.1063/1.3027514
View Table of Contents: http://jcp.aip.org/resource/1/JCPSA6/v129/i21
Published by the American Institute of Physics.

Simulations of the emission spectra of fac-tris(2-phenylpyridine) iridium and Duschinsky rotation effects using the Herman–Kluk semiclassical initial value representation method

Yinghua Wu[a] and Jean-Luc Brédas[b]
School of Chemistry and Biochemistry and Center for Organic Photonics and Electronics, Georgia Institute of Technology, 901 Atlantic Drive NW, Atlanta, Georgia, 30332-0400, USA

(Received 4 September 2008; accepted 22 October 2008; published online 4 December 2008)

The phosphorescent emission spectra of fac-tris(2-phenylpyridine) iridium [fac-Ir(ppy)$_3$] due to the lowest triplet T_1 and T_2 states are simulated using the harmonic oscillator approximation for the S_0, T_1, and T_2 potential energy surfaces (PESs) and taking the Duschinsky rotation into account. The simulations involve the propagation of 177-dimensional wave packets on the coupled PES according to the Herman–Kluk (HK) semiclassical (SC) initial value representation (IVR) method. The HK SC-IVR method is employed because of its accuracy for the PES with mode mixing and its efficiency in dealing with coupled degrees of freedom for large systems. The simulated emission spectrum due to T_1 reproduces the structures of the emission spectra observed experimentally, while T_2 is found very unlikely to participate in the phosphorescent emission. Although the effect of the Duschinsky mode mixing is small for the T_1 state, neglecting it blueshifts the spectrum due to the T_2 state by 800 cm^{-1} and changes the relative intensities, indicating that the importance of the Duschinsky rotation is rather unpredictable and should not be overlooked. The present simulations demonstrate that the simple harmonic oscillator approximation combined with the Duschinsky rotation can adequately describe the photophysics of fac-Ir(ppy)$_3$ and that the HK SC-IVR method is a powerful tool in studies of this kind. © *2008 American Institute of Physics*.
[DOI: 10.1063/1.3027514]

I. INTRODUCTION

Ir(III) compounds, especially fac-Ir(ppy)$_3$ (ppy =2-phenyl pyridine anion)[1–14] shown in Fig. 1 and other substituted complexes,[15–18] have attracted much research interest due to their application in phosphorescent organic light-emitting diodes (OLEDs).[19–21] As the purity of the emitted colors is one of the most important features in display applications, the emission properties of these materials have been extensively studied both experimentally and theoretically. While narrow and intense emission spectra lead to vibrant, saturated colors, organic emitters usually display broad emission spectra. Thus, the shape of the spectra is a practical concern in designing new light-emitting organic molecules, and a deeper understanding of the factors affecting it requires detailed investigations at the molecular level. In this work, we report the first calculation of the phosphorescent emission spectra of fac-Ir(ppy)$_3$, in which there is explicit treatment of the Duschinsky rotation effect using the Herman–Kluk (HK) semiclassical initial value representation (SC-IVR) method.[22,23] The method described here is general and can be easily implemented for other systems.

The calculation of the emission spectra of large organic molecules is a challenging problem. At the most fundamental level of theory, it requires the determination of accurate potential energy surfaces (PESs) from *ab initio* computations for both the ground and excited states in order to evaluate the overlaps among the various vibronic states. This task is clearly prohibitive without using parallel-mode and harmonic approximations except for very small molecules. In general, the harmonic approximation cannot give a reliable description of chemical processes, especially in instances that involve bond breaking or major changes in bond orders, in which case a double-well shaped PES is often needed, such as for the description of intramolecular proton transfer reactions.[24,25] However, for light-emitting applications, the emitters should not undergo large geometry changes, which could be detrimental to the stability and longevity of the devices. Therefore, the harmonic approximation is expected to model adequately the PES in these cases. This is confirmed by earlier electronic structure calculations on fac-Ir(ppy)$_3$, which show that the geometrical differences between the optimized ground state and the triplet states remain moderate;[6,14] also in our calculations, the energies for the S_0 state given by the harmonic approximation at the T_1 and T_2 optimized geometries are within 0.01 eV of the *ab initio* results, indicating that the anharmonic terms can be safely ignored.

Adopting the harmonic approximation implies that the underlying degrees of freedom are the normal modes. Although the geometrical changes during the radiative process are small, the electronic density distributions for the triplet states and the ground singlet state are different, as confirmed by both theoretical calculations[6,12,14] and experiments[7,8] showing that the emitting state has a metal-to-ligand charge-transfer character. This results in different vibrational normal

[a]Electronic mail: yinghua.wu@chemistry.gatech.edu.
[b]Electronic mail: jean-luc.bredas@chemistry.gatech.edu.

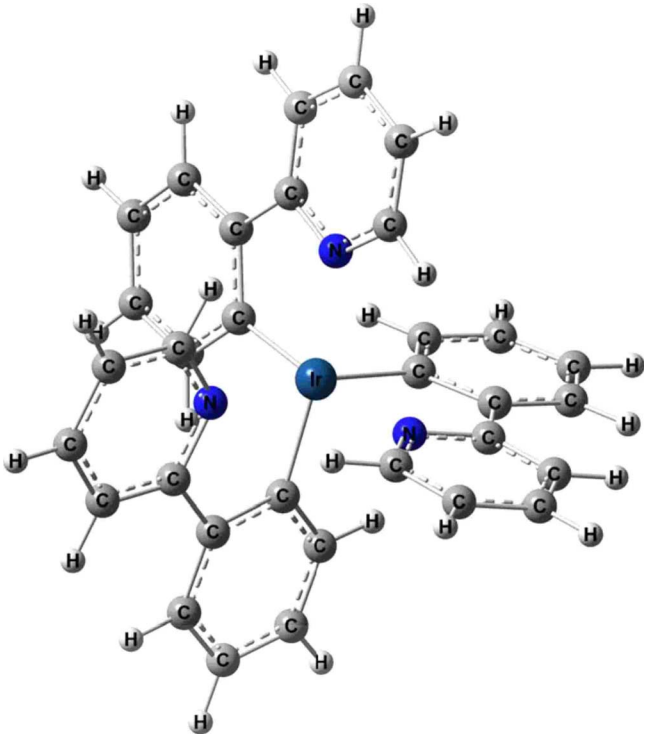

FIG. 1. (Color online) Structure of fac-Ir(ppy)$_3$ molecule.

modes for the ground state and the excited states, which casts doubt on the validity of the parallel-mode approximation. If one uses the normal modes of the ground state as the intrinsic degrees of freedom, the excited-state PES becomes coupled, and vice versa. This mode mixing is often referred to as the Duschinsky rotation effect.[26–30] Although it is still possible to compute the overlaps among different vibronic states recursively[31–35] to perform a sum-over-state analysis,[36–40] such a task is by no means affordable for organic emitters as the number of the vibronic states grows rapidly with the number of atoms. Therefore, here, we have chosen to take a quantum-dynamical approach[41–45] and to calculate the emission spectra by propagating the lowest vibrational wave packet of the excited triplet states on the S_0 PES, followed by Fourier transformation of the autocorrelation functions. Also, we employ the normal modes of the excited state as the underlying degrees of freedom so that the initial wave function is separable and we let the dynamics handle the coupled degrees of freedom.

Over the past decade, significant progress has been made in developing quantum-mechanical and SC methods for the simulations of quantum-dynamical processes in real time.[44,46–87] The core problem is to solve the time-dependent Schrödinger equation (TDSE). Recently, a few quantum-dynamical methods based on the coherent-state representations have emerged as feasible means to deal with large systems, such as the matching pursuit split operator Fourier transform method developed by Wu and Batista[46,47] or the coupled coherent-state method developed by Shalashilin *et al.*[48,49] Their applications include systems involving as many as 35 degrees of freedom.[25,88] However, certain implementations of these methods might not be as straightforward as the SC-IVR methods when applied to specific problems of interest, such as the model Hamiltonian considered in this work, where the degrees of freedom are significantly coupled. In fact, treating coupled degrees of freedom remains a major challenge for quantum-dynamical simulations. In this regard, the HK SC-IVR method[22,23] is particularly attractive. Instead of dealing with wave functions directly, the HK SC-IVR method runs a swamp of trajectories according to classical mechanics, each representing a coherent-state basis function. The time-evolved wave functions are obtained by summing up the time-evolved coherent states multiplied by the corresponding weights and coefficients. Thus, the coupled degrees of freedom are conveniently treated by the evolution of the classical trajectories. The HK SC-IVR method is also ideally suited for the system described here, since it has been shown that the method is uniformly accurate with respect to any time for harmonic oscillator kind of potential surfaces independently of how the degrees of freedom are coupled.[89–92] The error only comes from the initial Monte Carlo sampling, which can be easily fixed by adding more trajectories, and the error does not propagate.

II. METHODOLOGY

A. PES and Duschinsky rotation matrix

fac-Ir(ppy)$_3$ is known to be an efficient green emitter[19–21] and it is generally accepted that the phosphorescent emission is largely due to the T_1 electronic state.[7,8,14] To demonstrate the capabilities of the method described here and to evaluate the importance of the Duschinsky rotation effect, we also consider the T_2 state. Studies of higher-lying excited states are important for organic molecules that could be used for white OLEDs, as emissions from different states could contribute to broad emission spectra giving a white color. Here, we only consider a single fac-Ir(ppy)$_3$ molecule in vacuum and model the PESs for the S_0, T_1, and T_2 states by harmonic oscillators. While this constitutes a simple approximation with respect to real device configurations, we believe it is the first attempt to address the emission spectra of such large molecules by treating the Duschinsky rotation effect explicitly with a full quantum-dynamical method.

Throughout this paper, we adopt the mass-weighted coordinates for both Cartesian coordinates and normal modes and use the subscripts 0, 1, and 2 to refer to the S_0, T_1, and T_2 states, respectively. The PESs are expanded by harmonic oscillators around the optimized geometries of the different electronic states:

$$V_{S_0}(\mathbf{x}) = \sum_{i=1}^{N} \frac{1}{2} m_{\mathrm{H}} \omega_{0i}^2 x_i^2,$$

$$V_{T_1}(\mathbf{y}) = \sum_{i=1}^{N} \frac{1}{2} m_{\mathrm{H}} \omega_{1i}^2 y_i^2 + e_1, \tag{2.1}$$

$$V_{T_2}(\mathbf{z}) = \sum_{i=1}^{N} \frac{1}{2} m_{\mathrm{H}} \omega_{2i}^2 z_i^2 + e_2,$$

where $N=177$ is the number of normal modes, m_{H} is the hydrogen mass, and ω are the normal-mode frequencies. We

have taken the energy of the optimized S_0 state as the reference and $e_{1(2)}$ denotes the 0-0 transitions between the $T_{1(2)}$ and S_0 states. The variables $\mathbf{x}$, $\mathbf{y}$, and $\mathbf{z}$ in Eq. (2.1) are the displacements in normal modes relative to the corresponding optimized S_0, T_1, and T_2 geometries. To convert a random geometry $\mathbf{q}$ into $\mathbf{x}$, $\mathbf{y}$, and $\mathbf{z}$, one can simply project the displacements onto the three sets of normal modes:

$$\begin{aligned}\mathbf{x} &= \mathbf{L}_0^T(\mathbf{q}-\mathbf{q}_0),\\ \mathbf{y} &= \mathbf{L}_1^T(\mathbf{q}-\mathbf{q}_1),\\ \mathbf{z} &= \mathbf{L}_2^T(\mathbf{q}-\mathbf{q}_2),\end{aligned} \tag{2.2}$$

where $\mathbf{q}_{0(1,2)}$ are the optimized geometries in Cartesian coordinates and the matrices $\mathbf{L}$ have 183×177 dimensions with each column vector representing a normal mode, which can be obtained by diagonalizing the mass-weighted Hessian matrices.

To calculate the emission spectrum of $Ir(ppy)_3$ due to the T_1 or T_2 state, one can propagate the lowest vibrational wave function of the excited electronic state on the ground-state PES, followed by a Fourier transform of the autocorrelation function.[41–45] To carry out the calculations, the wave functions and the PES must be cast on the same coordinates; therefore, it is necessary to relate the different sets of variable in Eq. (2.2). Had we used the parallel-mode approximation, we would have the same $\mathbf{L}$ in Eq. (2.2), and the only differences among $\mathbf{x}$, $\mathbf{y}$, and $\mathbf{z}$ would be constant vectors. In this case, the system would be completely separable. Although the parallel-mode approximation is frequently used in Frank–Condon analyses and other quantum-dynamical studies involving many degrees of freedom due to the complexity involved, the assumption that the normal modes are the same for different electronic states is in general not valid as the electron densities are different. It is straightforward to convert one set of variables to another. Rearranging Eq. (2.2) yields

$$\begin{aligned}\mathbf{x} &= \mathbf{L}_0^T\mathbf{L}_1\mathbf{y} + \mathbf{L}_0^T(\mathbf{q}_1-\mathbf{q}_0),\\ \mathbf{x} &= \mathbf{L}_0^T\mathbf{L}_2\mathbf{z} + \mathbf{L}_0^T(\mathbf{q}_2-\mathbf{q}_0),\end{aligned} \tag{2.3}$$

where $D\equiv\mathbf{L}_0^T\mathbf{L}_{1(2)}$ is the so-called Duschinsky rotation matrix. A glance at the largest absolute values for each row of the Duschinsky matrix will reveal how different the two sets of normal modes are and to what extent the modes are mixed. From our calculations, these values almost evenly range from 0.6 to 0.95 indicating that the normal modes of the excited states are significantly mixed in terms of those of the ground electronic state. Therefore, it is necessary to treat the mode mixing explicitly in quantum-dynamical calculations. For numerical convenience, we use the normal modes of the excited states as the underlying degrees of freedom so that the initial wave functions are uncoupled Gaussian wave functions, and the ground-state PESs are functions with coupled degrees of freedom:

$$\begin{aligned}V_{S_0}(\mathbf{y}) &= \sum_{i=1}^{N}\frac{1}{2}m_{\mathrm{H}}\omega_{0i}^2[\mathbf{L}_0^T\mathbf{L}_1\mathbf{y}+\mathbf{L}_0^T(\mathbf{q}_1-\mathbf{q}_0)]_i^2,\\ V_{S_0}(\mathbf{z}) &= \sum_{i=1}^{N}\frac{1}{2}m_{\mathrm{H}}\omega_{0i}^2[\mathbf{L}_0^T\mathbf{L}_2\mathbf{z}+\mathbf{L}_0^T(\mathbf{q}_2-\mathbf{q}_0)]_i^2\end{aligned} \tag{2.4}$$

where the subscript i indicates the ith element of the vector in square brackets. Although the PESs in Eq. (2.4) are harmonic in nature, an analytical quantum-dynamics propagator is not yet available due to the complexity involved with mode mixing. Alternatively, one can use the normal modes of the ground state as the underlying degrees of freedom, in which case the S_0 PES will be uncoupled harmonic oscillators, but the initial wave packet will be a function of coupled degrees of freedom. In either scenario, a simple closed form for the propagation of the wave functions is not available.

B. HK SC-IVR method

The HK SC-IVR method[22,23] was developed as an alternative way to solve the TDSE by running classical trajectories and incorporating quantum-dynamical effects by a phase factor for each trajectory. For nonchaotic systems, these trajectories can be efficiently sampled by Monte Carlo techniques, thus bypassing the usual exponential scaling that is often associated with full quantum-dynamical methods. It has been shown that the HK SC-IVR method is accurate to the first order of $\hbar$ and that the error is $O(\hbar^2)$ for general cases. It is, however, accurate for the PESs whose third derivatives with respect to displacements vanish, as is the case in Eq. (2.4). The derivation was first given by Kay,[89–91] and a more detailed derivation for multidimensional cases can be found in Ref. 92.

In the HK SC-IVR method, each trajectory represents an evolving frozen Gaussian basis function:

$$\langle\mathbf{q}|\mathbf{R}_t,\mathbf{P}_t\rangle = \left|\frac{\boldsymbol{\gamma}}{\pi}\right|^{N/4}\exp\left[-\frac{1}{2}(\mathbf{q}-\mathbf{R}_t)^T\boldsymbol{\gamma}(\mathbf{q}-\mathbf{R}_t) + \frac{i}{\hbar}\mathbf{P}_t(\mathbf{q}-\mathbf{R}_t)\right], \tag{2.5}$$

where $\mathbf{R}_t$ and $\mathbf{P}_t$ are the position and momentum parameters of a trajectory at time t evolved from $(\mathbf{R}_0,\mathbf{P}_0)$ at time zero following classical equations of motion, $d\mathbf{R}_t/dt=\mathbf{P}_t/m$, $d\mathbf{P}_t/dt=-\nabla V(\mathbf{R}_t)$, and $\boldsymbol{\gamma}$ is a diagonal matrix consisting of the width parameters for each degrees of freedom. We have used the same mass m for the modes to be consistent with the use of mass-weighted coordinates. The time-evolved wave function $|\psi_t\rangle$ is expressed as

$$\langle\mathbf{q}|\psi_t\rangle = \left(\frac{1}{2\pi\hbar}\right)^d\int d\mathbf{R}_0\int d\mathbf{P}_0\langle\mathbf{q}|\mathbf{R}_t,\mathbf{P}_t\rangle C(\mathbf{R}_0,\mathbf{P}_0,t)\exp \times[iS(\mathbf{R}_0,\mathbf{P}_0,t)/\hbar]\langle\mathbf{R}_0,\mathbf{P}_0|\psi_0\rangle, \tag{2.6}$$

where d is the dimensionality, $|\psi_0\rangle$ is the initial wave function, $S(\mathbf{R}_0,\mathbf{P}_0,t)$ is the classical action $\int_0^t(T-V)d\tau$, and $C(\mathbf{R}_0,\mathbf{P}_0,t)$ is the HK coefficient given by

$$C(\mathbf{R}_0,\mathbf{P}_0,t)=\left|\frac{1}{2}\left(\boldsymbol{\gamma}^{-1}\frac{\partial\mathbf{P}_t}{\partial\mathbf{P}_0}\boldsymbol{\gamma}+\frac{\partial\mathbf{R}_t}{\partial\mathbf{R}_0}-i\hbar\frac{\partial\mathbf{R}_t}{\partial\mathbf{P}_0}\boldsymbol{\gamma}-\frac{1}{i\hbar}\boldsymbol{\gamma}^{-1}\frac{\partial\mathbf{P}_t}{\partial\mathbf{R}_0}\right)\right|^{1/2}. \quad (2.7)$$

The matrices inside the determinant in Eq. (2.7) can be propagated along the trajectory according to

$$\begin{aligned}
&\frac{d}{dt}\frac{\partial\mathbf{R}_t}{\partial\mathbf{R}_0}=\frac{1}{m}\frac{\partial\mathbf{P}_t}{\partial\mathbf{R}_0},\\
&\frac{d}{dt}\frac{\partial\mathbf{P}_t}{\partial\mathbf{R}_0}=-\nabla^2V(\mathbf{R}_t)\frac{\partial\mathbf{R}_t}{\partial\mathbf{R}_0},\\
&\frac{d}{dt}\frac{\partial\mathbf{R}_t}{\partial\mathbf{P}_0}=\frac{1}{m}\frac{\partial\mathbf{P}_t}{\partial\mathbf{P}_0},\\
&\frac{d}{dt}\frac{\partial\mathbf{P}_t}{\partial\mathbf{P}_0}=-\nabla^2V(\mathbf{R}_t)\frac{\partial\mathbf{R}_t}{\partial\mathbf{P}_0}.
\end{aligned} \quad (2.8)$$

The calculation of the HK coefficient constitutes the most time-consuming part of the HK SC-IVR method. Following Guallar *et al.*,[93] it can be simplified by combining the matrices as follows:

$$\begin{aligned}
&\mathbf{A}_t=\frac{\partial\mathbf{R}_t}{\partial\mathbf{R}_0}-i\hbar\frac{\partial\mathbf{R}_t}{\partial\mathbf{P}_0}\boldsymbol{\gamma},\\
&\mathbf{B}_t=-i\hbar\boldsymbol{\gamma}\left(\boldsymbol{\gamma}^{-1}\frac{\partial\mathbf{P}_t}{\partial\mathbf{P}_0}\boldsymbol{\gamma}-\frac{1}{i\hbar}\boldsymbol{\gamma}^{-1}\frac{\partial\mathbf{P}_t}{\partial\mathbf{R}_0}\right),
\end{aligned} \quad (2.9)$$

so that

$$C(\mathbf{R}_0,\mathbf{P}_0,t)=\left|\frac{1}{2}\left(\mathbf{A}_t-\frac{\mathbf{B}_t}{i\hbar\boldsymbol{\gamma}}\right)\right|^{1/2}, \quad (2.10)$$

where $d\mathbf{A}_t/dt=\mathbf{B}_t/m$ and $d\mathbf{B}_t/dt=-\nabla^2V\mathbf{A}_t$. The HK coefficient is an oscillatory function of time and normally becomes more oscillatory with increasing degrees of freedom. As Kay[89,94] pointed out, the time increment for propagating the trajectories should be small enough and the sign should be checked frequently to ensure that the coefficient is continuous.

To calculate the autocorrelation function, one just needs to replace $\langle\mathbf{q}|$ with the initial wave function $\langle\psi_0|$ in Eq. (2.6). The implementation of the HK SC-IVR method includes the following easy steps: (i) sampling of a trajectory according to the magnitude of the overlap $|\langle\mathbf{R}_0,\mathbf{P}_0|\psi_0\rangle|$; (ii) propagating this trajectory according to classical equations of motion and calculating the HK coefficient as described in Eq. (2.10); and (iii) along the time evolution, calculating the overlaps between the time-evolved basis function and the initial wave function and multiplying all the phase factors in Eq. (2.7). This process should be repeated as many times as necessary so that the contributions from all the trajectories will converge.

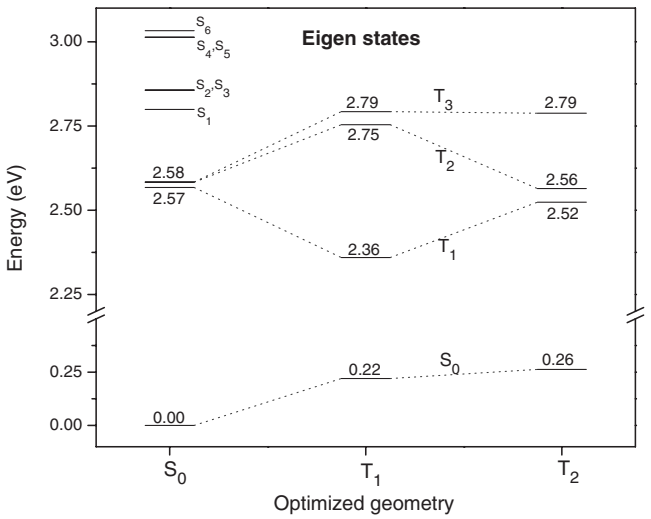

FIG. 2. The energies of various eigenstates of fac-Ir(ppy)$_3$ molecule at the S_0, T_1, and T_2 optimized geometries. The dotted lines are there to indicate the same states.

III. RESULTS

A. Structures and Duschinsky rotation matrices

The geometric structures of fac-Ir(ppy)$_3$ were fully optimized without symmetry constraints in the singlet ground-state S_0 and first (T_1) and second (T_2) triplet states using the TURBOMOLE package[95] at the density functional theory (DFT) level with the B3LYP functional. The def-TZVP basis set was used for Ir and def-SVP basis set for the other light atoms. The energies of various eigenstates at these optimized geometries are shown in Fig. 2, where we have included the third (T_3) triplet state and the lowest six singlet (S_{1-6}) excited states. The optimized geometries were rotated to the same axis before frequency analysis and normal-mode calculations. Since our main purpose is to calculate the phosphorescence emission spectra, we will only briefly discuss the geometric-structure calculations. Table I compares the Ir–N and Ir–C bond lengths in the S_0, T_1, and T_2 optimized geometries; those reported in earlier experiments and calculations are included as well. Although there are small differences in Ir–N bond lengths of about 0.1 Å between our calculations and the crystal structures, such differences are not surprising since the calculations are carried out on a single molecule in vacuum. Comparing with other calculations, the corresponding bond lengths are all within 0.03 Å of each other. Our geometry optimizations indicate that the optimized S_0 structure is very close to C_3 symmetry, while for the optimized T_1 and T_2 states, the ppy ligands are slightly displaced with two ligands pushed away from the Ir atom and one pulled closer. Our calculations also underline that the geometry differences between the optimized T_2 and T_1 states are much smaller than between T_1 and S_0.

Since the optimized T_1 and T_2 geometries are somewhat displaced from the optimized S_0 geometry, it is important to validate the harmonic approximation for the S_0 PES given in Eq. (2.1). While it is impossible to check every point around the optimized S_0 geometry, meaningful evaluations can be gained at the optimized T_1 and T_2 geometries by examining

TABLE I. DFT-B3LYP bond lengths (Å) in the optimized S_0, T_1, and T_2 states (the numbers in parentheses denote the various ppy ligands).

	T_2	T_1		S_0				
	Calc.	Calc.	Calc.[a]	Calc.	Calc.[a]	Calc.[b]	Expt.[c]	Expt.[d]
Ir–N(1)	2.155	2.139	2.116	2.179	2.151	2.167	2.086	2.132
Ir–C(1)	2.013	2.005	2.000	2.035	2.035	2.035	2.034	2.024
Ir–N(2)	2.215	2.201	2.176	2.179	2.154	2.167	2.086	2.132
Ir–C(2)	2.008	2.027	2.048	2.035	2.035	2.035	2.034	2.024
Ir–N(3)	2.203	2.196	2.169	2.179	2.153	2.167	2.086	2.132
Ir–C(3)	2.069	2.049	2.040	2.035	2.035	2.035	2.034	2.024

[a]Reference 14, B3LYP/Lanl2DZ.
[b]Reference 6, B3LYP/Lanl2DZ.
[c]Reference 8, x ray.
[d]Reference 2, x ray.

the reorganization energies on the S_0 PES, i.e., the energy difference on the S_0 PES between the optimized $T_{1(2)}$ and S_0 geometries. Direct evaluations of the reorganization energies give values of 0.220 eV (T_1) and 0.263 eV (T_2), while the values calculated within the harmonic approximation are 0.231 eV (T_1) and 0.273 eV (T_2), respectively. The small differences of 0.01 eV mean that the optimized T_1 and T_2 geometries are well within the harmonic region, which comes as not much of a surprise since there is no chemical reaction that could cause bond breaking or major changes in bond orders during the radiation process. Figure 3 shows the displacements in terms of the S_0 normal modes at the optimized T_1 and T_2 geometries relative to the optimized S_0 geometry. The normal modes are indexed with increasing frequencies, and the same indexing is used for the other figures. Figure 3 suggests that the harmonicity can be attributed to the fact that most of the large displacements take place for low-frequency modes; thus, even if the potential curves for certain normal modes are not closely harmonic, those deviations do not significantly add up to the reorganization energy. The general structure of fac-Ir(ppy)$_3$, which is close to the C_3 symmetry, can also help in maintaining harmonicity. It will

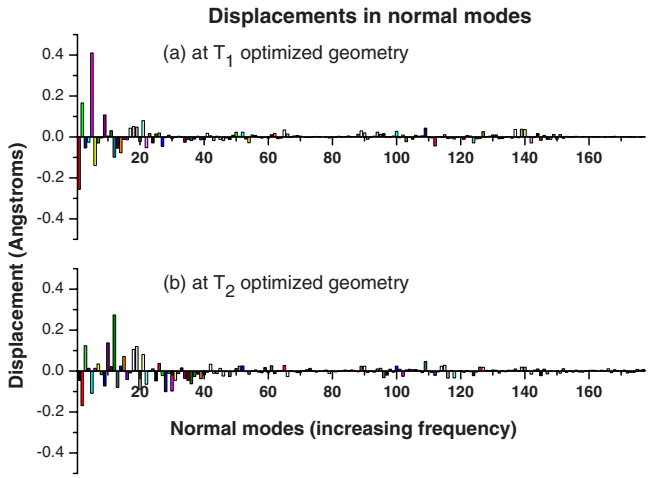

FIG. 3. (Color online) Displacements in terms of the 177 S_0 normal modes at the optimized (a) T_1 and (b) T_2 geometries relative to the optimized S_0 geometry (the frequencies of the selected modes are given in Table II).

be interesting to evaluate whether the harmonic approximation remains as good when Ir is surrounded by different ligands (heteroleptic complexes).

Previous experiments[7,8] and calculations[6,14] have shown that the emitting T_1 state has a metal-to-ligand charge-transfer character. The shift in electron density not only causes the geometry changes but also alters the strength of the bonds, resulting in frequency shifts and mixing of the normal modes. For comparison, some frequencies are collected in Table II for the three states. Figures 4 and 5 show the contour maps of the absolute values of the Duschinsky rotation matrices for S_0-T_1 and S_0-T_2, respectively, along with the maximum absolute values for each row. According to Eq. (2.2), these maximum values represent the overlaps between the S_0 normal modes with the corresponding $T_{1(2)}$ normal modes, and therefore serve as a measure of how much the S_0 normal modes remain themselves on the T_1 and T_2 states. The average values are 0.795($\pm$0.126) for the S_0-T_1 matrix and 0.730($\pm$0.148) for the S_0-T_2 matrix, where the numbers in parentheses are the standard deviations. The smaller average and larger deviation from the S_0-T_2 matrix indicate more mode mixing in the T_2 state than in the T_1 state, which is consistent with the fact that the electronic wave functions for higher excited states are expected to deviate more significantly from the ground state. The contour maps show that the Duschinsky rotation matrices are almost diagonal, which means that most mode mixing occurs among modes with similar frequencies. Considering the off-diagonal elements of the contour maps, it is also clear that the mode mixing between the S_0 and T_2 states is more complex and involves a larger number of middle- and high-frequency modes.

B. Emission spectra due to the T_1 and T_2 states

Following Heller,[41–43] the emission spectrum $\sigma(\omega)$ due to the T_1 or T_2 electronic state is computed as the Fourier transform of the survival amplitudes $\xi(t)$:

$$\sigma(\omega) = C\omega^3 \int_0^\infty dt\, \mathrm{Re}[\xi(t)] e^{i(-\omega+\varepsilon_0)t}, \tag{3.1}$$

where $\xi(t) = \langle \Psi_0 | \Psi_t \rangle$ is the autocorrelation function and ε_0 is the 0-0 transition corresponding to the transition from the

TABLE II. Frequencies (cm^{-1}) of some selected normal modes for the S_0, T_1, and T_2 states.

Mode	S_0	T_1	T_2
3	32.8	37.5	35.9
6	49.6	50.6	52.0
9	86.3	87.6	89.0
12	125.4	122.5	123.8
15	167.3	168.3	170.7
18	204.9	202.4	196.2
21	259.6	246.1	251.0
24	276.8	276.0	272.4
27	302.3	301.4	329.2
30	384.7	383.9	382.8
33	436.3	434.9	435.1
36	461.7	454.9	454.2
39	490.2	487.5	486.1
42	519.8	514.2	526.1
45	579.1	577.6	577.0
48	643.5	643.7	644.0
51	653.6	654.2	652.9
54	682.6	680.6	681.1
57	755.2	729.3	748.7
60	760.5	753.4	756.6
63	772.5	768.1	769.5
66	777.5	775.2	776.8
69	830.8	828.7	828.7
72	894.0	891.8	893.3
75	904.8	905.5	910.1
78	971.9	957.8	965.3
81	985.3	972.6	989.0
84	1017.6	993.2	1007.1
87	1020.0	1018.7	1021.7
90	1026.1	1023.0	1025.8
93	1036.2	1028.1	1033.8
96	1056.3	1036.3	1048.0
99	1074.5	1072.6	1074.3
102	1081.7	1080.1	1084.6
105	1125.4	1122.3	1125.9
108	1145.3	1143.6	1143.5
111	1166.8	1166.3	1168.3
114	1174.8	1173.8	1182.4
117	1261.3	1258.4	1264.2
120	1295.9	1295.2	1300.1
123	1323.5	1325.4	1326.4
126	1329.8	1329.0	1333.6
129	1348.4	1368.1	1356.1
132	1448.8	1435.9	1447.5
135	1468.0	1466.5	1465.3
138	1479.9	1481.3	1482.6
141	1509.3	1506.6	1511.8
144	1594.4	1552.6	1583.3
147	1615.4	1594.3	1615.8
150	1641.3	1633.3	1637.9
153	1653.3	1655.7	2581
156	3157.3	3164.0	3170.4
159	3166.9	3178.0	3177.8
162	3183.1	3184.0	3186.0
165	3185.6	3187.1	3188.3
168	3191.3	3196.3	3196.3
171	3198.3	3201.4	3207.8
174	3211.9	3212.0	3216.2
177	3217.8	3219.0	3225.6

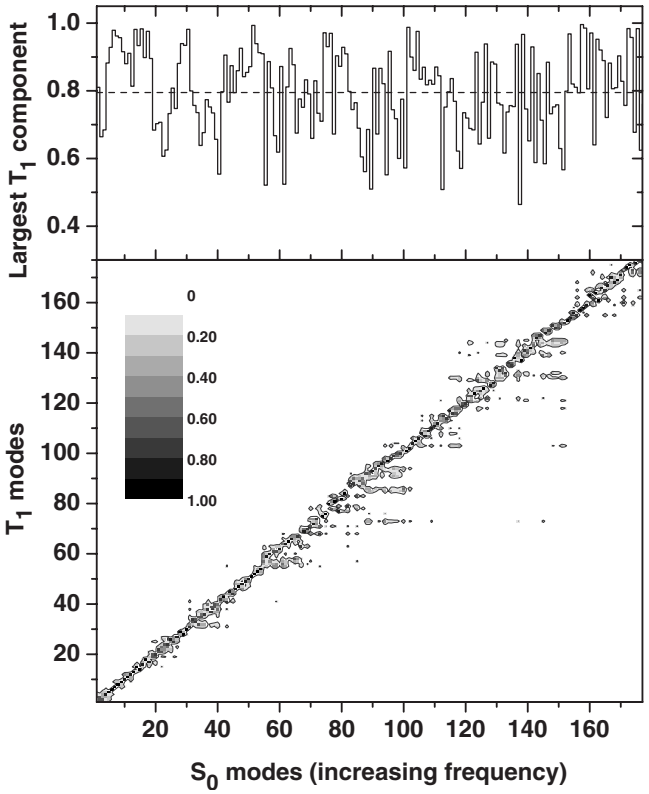

FIG. 4. Contour map of the Duschinsky rotation matrix (lower panel) for the S_0 and T_1 normal modes along with the largest absolute value (upper panel) for each row. The average of the largest absolute values is shown as the dashed line. Gray colors are filled between different contour levels and one contour curve is shown at the level of 0.1.

optimized $T_{1(2)}$ state to the optimized S_0 state. Since the geometry of the molecule does not change significantly during the radiation process, the constant transition-dipole approximation is adopted implicitly to simplify the calculations. Thus, $|\Psi_0\rangle$ is the initial wave packet for the lowest vibrational level on the $T_{1(2)}$ state:

$$\langle \mathbf{x}|\Psi_0\rangle = \prod_{j=1}^{177} \left(\frac{m_{\mathrm{H}}\omega_j}{\pi}\right)^{1/4} \exp\left(-\frac{1}{2}m_{\mathrm{H}}\omega_j x_j^2\right), \tag{3.2}$$

where ω_j are the frequencies of the normal modes (we have used the same mass m_{H} for the normal modes due to the use of mass-weighted coordinates). $|\Psi_t\rangle = \langle\Psi_0|e^{-i\hat{H}t/\hbar}|\Psi_0\rangle$ is the time-evolved wave function obtained by solving the TDSE on the S_0 PES given by Eq. (2.4) based on the HK SC-IVR method and the procedure described in Sec. II B.

In order to study the effect of mode mixing, the emission spectra are calculated using both the Duschinsky rotation matrices and the identity matrix as substitute; in the latter case, the system becomes totally separable and the autocorrelation functions can be evaluated analytically as is done in this work. To improve the efficiency of Monte Carlo sampling, a threshold of 1.0×10^{-10} is set for the sampling amplitude and a trajectory is rejected if the absolute value of the overlap with the initial wave function is lower than the threshold. The wave functions are propagated for the time necessary for the spectra to no longer change. Since the HK coefficient is a highly oscillatory function of time, a small

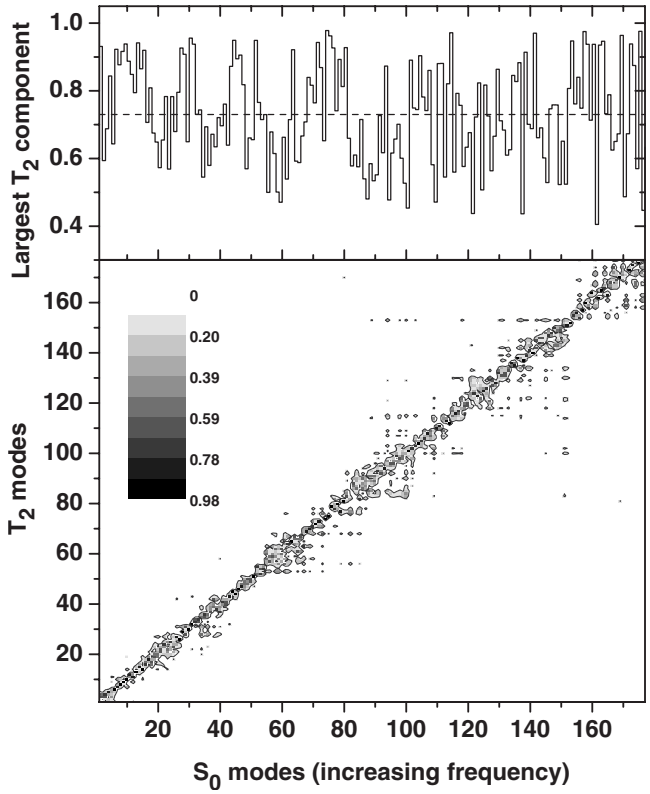

FIG. 5. Contour map of the Duschinsky rotation matrix (lower panel) for the S_0 and T_2 normal modes along with the largest absolute value (upper panel) for each row. The average of the largest absolute values is shown as the dashed line. Gray colors are filled between different contour levels and one contour curve is shown at the level of 0.1.

time increment has to be used to ensure its continuance. We found that (i) a time increment of 0.05 fs, (ii) a total propagation time of 200 fs, and (iii) 300 000 trajectories provide the convergence of the autocorrelation functions and the spectra. According to the Fourier transform theory,[44] the use of such parameters can accommodate a bandwidth of 41.3 eV and provide a resolution of 0.01 eV.

Figures 6 and 7 compare the amplitudes of the autocorrelation functions obtained with and without the Duschinsky matrices due to the T_1 and T_2 states, respectively. Since the autocorrelation functions are too oscillatory and the phases obtained with and without the Duschinsky matrix are virtually the same across the whole range, only the amplitudes are shown here for better comparison. In both figures, the amplitudes obtained with the Duschinsky matrices are slightly larger than those obtained without them. This suggests that the mode mixings actually bring the geometries closer to the original Frank–Condon configurations for fac-Ir(ppy)$_3$ or, in other words, that negligence of the Duschinsky matrix overestimates the molecular motions. Figures 6 and 7 also show that the absolute values of the autocorrelation functions drop to 15% in only 10–15 fs, indicating that the molecule quickly reorganizes after photon emission. There are significant differences between the autocorrelation functions for T_1 and T_2 in that the survival amplitudes of the T_1 state show many more pronounced recurrences and oscillations than those of the T_2 state. We can infer that the time-evolved wave functions of the T_1 state is closer to the bottom of the S_0 PES and bounce around with more strength, in accordance with the fact that the reorganizations for the optimized T_1 and T_2 geometries on the S_0 ground state are 0.23 and 0.27, respectively. Hence, it is expected that the lower-lying vibronic levels of the S_0 state participate more in the emission processes due to the T_1 state. This is clearly demonstrated in the simulated phosphorescent emission spectra due to the T_1 and T_2 states as shown in Figs. 8 and 9, respectively. It is, however, interesting to see that the small difference of 0.04 eV in reorganization energies can make so much difference.

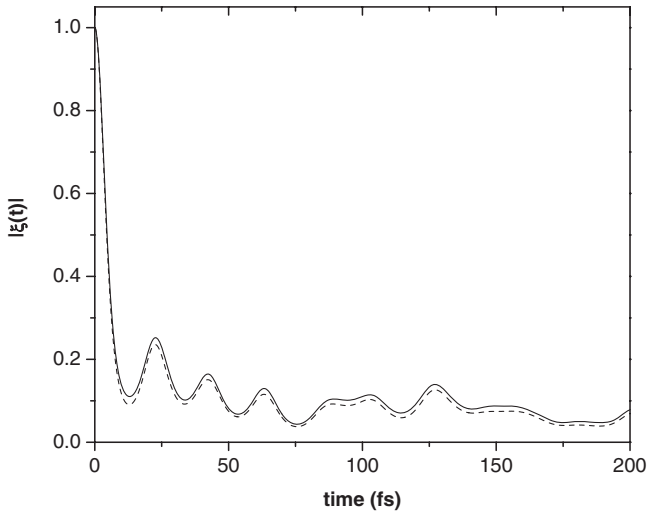

FIG. 6. Comparison of amplitudes for the autocorrelation function for the T_1 initial wave function with (solid line) and without (dashes) Duschinsky mode mixing.

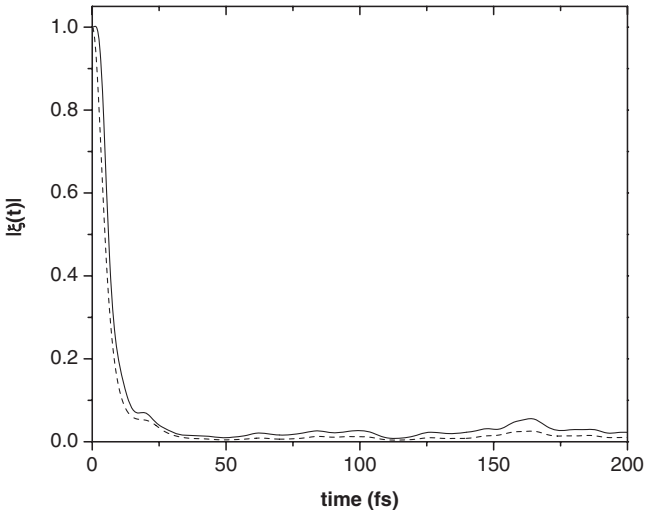

FIG. 7. Comparison of amplitudes for the autocorrelation function for the T_2 initial wave function with (solid line) and without (dashes) Duschinsky mode mixing.

In Figs. 8 and 9, we have taken the dephasing effect due to the interaction between the Ir(ppy)$_3$ molecule and its surrounding into account by multiplying the survival amplitudes $\xi(t)$ by the damping factor e^{-t/τ_2} before computing the Fourier transform according to Eq. (3.1). We have used $\tau_2 = 70$ fs for both Figs. 8 and 9. This procedure simply smoothens the calculated spectra (which no longer display sharp individual spikes) without shifting the positions of the

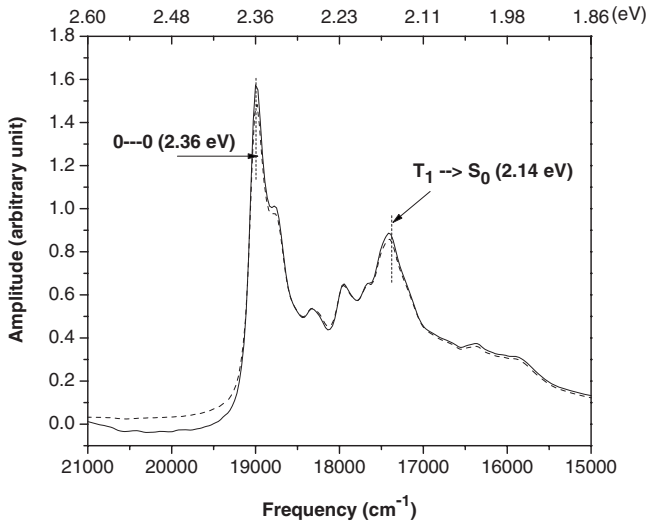

FIG. 8. Emission spectrum due to the T_1 state. The solid (dashed) line shows the result with (without) Duschinsky mode mixing. The 0-0 transition and the $T_1 \rightarrow S_0$ vertical transition are indicated. The energy axis goes from higher to lower values in order to provide an easier comparison with the experimental spectra in Refs. 7 and 8.

peaks. Figure 8 shows that there are two major peaks due to the T_1 state: one at 19 000 cm^{-1} (2.36 eV) perfectly corresponds to the 0-0 transition and the other at 17 400 cm^{-1} (2.16 eV) is very close to the $T_1 \rightarrow S_0$ vertical transition at 2.14 eV. On the other hand, the simulated emission from the T_2 state as shown in Fig. 9 presents only one major band at 19 000 cm^{-1} (2.36 eV), lying close to the $T_2 \rightarrow S_0$ vertical transition (2.30 eV). The differences in the profiles of the simulated emission spectra due to the T_1 and T_2 states demonstrate that a deeper understanding of the factors responsible for the features of the emission spectra requires detailed investigation at the molecular level.

With respect to the experimental spectra, the overall features of the simulated spectrum in Fig. 8 resemble those of the experimental single-crystal emission spectrum at room temperature, see Fig. 10(a). Our calculations reproduce the

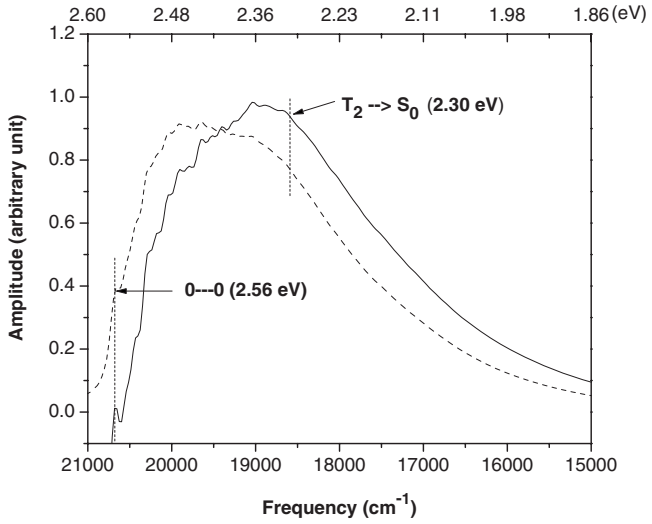

FIG. 9. Emission spectrum due to the T_2 state. The solid (dashed) line shows the result with (without) Duschinsky mode mixing. The 0-0 transition and the $T_2 \rightarrow S_0$ vertical transition are indicated.

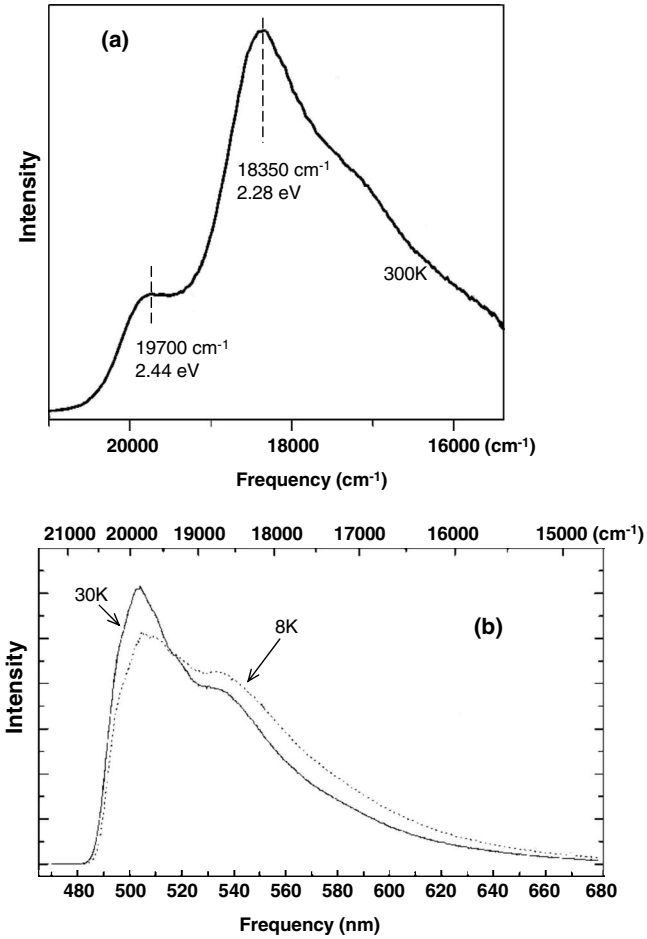

FIG. 10. (a) Experimental single-crystal emission spectrum of fac-$Ir(ppy)_3$ at $T=300$ K, adapted from Ref. 8. (b) Experimental emission spectra of fac-$Ir(ppy)_3$ in THF at selected temperatures, adapted from Ref. 7.

frequency range and the presence of two distinctive emission bands, in excellent agreement with the experimental spectrum. In comparison to the experimental emission bands at around 19 700 and 18 350 cm^{-1}, our results are systematically redshifted by about ~1000 cm^{-1} (~0.1 eV), which is well within differences between the results of the gas-phase calculations and condensed-phase experimental data. Our calculations indicate that the 0-0 band is more intense than the $T_1 \rightarrow S_0$ band, which is consistent with the experimental spectra collected at low temperatures in the 8–30 K range, as shown in Fig. 10(b).

Interestingly, temperature-dependent emission spectra for $Ir(ppy)_3$ dissolved in tetrahydrofuran (THF) indicate that the relative intensities for the two bands are inverted at room temperature (see Fig. 1 of Ref. 7). Since the relative intensities of the two major emission bands can vary greatly depending on the conditions, this has caused some difficulty in the assignment of the peaks. While the 18 350 cm^{-1} band has been generally identified as the $T_1 \rightarrow S_0$ transition and our simulation shows the same, the nature of the 19 700 cm^{-1} band has been somewhat unclear; it has been proposed to be due to the zero-field spin-orbital splittings of the T_1 state which, however, only amount to dozens of wave numbers[7,10] or caused by different surfaces of a crystal.[8] Unfortunately, including solvent molecules or more $Ir(ppy)_3$ molecules to

better simulate the real conditions at a high level of theory remains not feasible at present, and physical intuition is needed in interpreting the calculated and observed spectra. The main message of Fig. 8 is to illustrate that the 0-0 transition can be held accountable for the experimental band at 19 700 cm^{-1}, which corresponds to the calculated 19 000 cm^{-1} band. It is important to note that without calculating the whole spectrum based on the full quantum-dynamical approach, such assignments would not be possible from single-point calculations (earlier theoretical studies actually compared the calculated $T_1 \rightarrow S_0$ transition with the observed 19 800 cm^{-1} band[6,14]). It would be useful in future studies to include the temperature effect and consider the interactions with the surroundings to address the issue of relative intensities in different conditions.

Interestingly, the consideration of the Duschinsky rotation matrix causes little difference to the emission spectrum due to the T_1 state as shown in Fig. 8. This suggests either that the overall effect of the mode mixing smoothens the changes due to each individual mode or that the mixing is simply not significant enough.

However, the effect of mode mixing can be clearly seen from the T_2 emission spectra obtained with and without the Duschinsky rotation matrix, as shown in Fig. 9. Setting the Duschinsky matrix to identity causes the maximum emission to blueshift by 0.1 eV, a direct evidence of overestimating the molecular motions. Although the spectra are similar in shape, the relative intensities of the 0-0 and $T_2 \rightarrow S_0$ transition are modified. Due to the large number of modes involved, it is difficult to assess which modes play the most important roles. The difference in impact of the Duschinsky rotation matrix can be traced back to the more complex mode mixing seen for T_2, as demonstrated by the contour maps in Figs. 4 and 5. Comparing Figs. 8 and 9, we conclude that the impact of mode mixing is highly case dependent and that caution is required when employing the parallel-mode approximation.

Unlike the emission spectrum due to the T_1 mode, the emission from the T_2 state shows only one major band at 19 000 cm^{-1} (2.36 eV), roughly corresponding to the $T_2 \rightarrow S_0$ vertical transition, and the 0-0 transition 20 600 cm^{-1} (2.56 eV) is substantially weaker. If we were to adopt the same systematic blueshift of 1000 cm^{-1} as in the T_1 case, the corresponding 0-0 and $T_2 \rightarrow S_0$ transitions should be experimentally observed at about 21 600 and 19 550 cm^{-1}, respectively. Since the 21 600 cm^{-1} band has not been observed experimentally, this appears to rule out the possibility of emission from the T_2 state.

IV. SUMMARY

We have calculated the phosphorescent emission spectra of fac-Ir(ppy)$_3$ due to the T_1 and T_2 states based on the time-dependent approach according to the HK SC-IVR method. The calculations require constructing the PESs for the S_0, T_1, and T_2 states with the corresponding normal modes for each electronic state based on the harmonic approximation and treating the Duschinsky rotation effect explicitly. The calculations also involve propagating the lowest vibrational wave functions of the T_1 and T_2 electronic states on the S_0 PES. While the complexity inherent to mode mixing among 177 normal modes makes such a task not feasible with other quantum-dynamical methods, this is a case that can be treated accurately and efficiently by the HK SC-IVR method.

We have shown that the Duschinsky rotation effect has little effect on the emission spectrum from the T_1 state, while a stronger effect is seen for the emission from the T_2 state. Thus, our calculations clearly show that the Duschinsky rotation effect is case dependent and should not be overlooked. According to the calculated emission spectra, we have assigned the experimentally observed band at 18 350 cm^{-1} to the $T_1 \rightarrow S_0$ vertical transition. Our assignment of the 19 800 cm^{-1} band as the 0-0 $T_1 \rightarrow S_0$ transition differs from some earlier experimental and theoretical studies. We have also underlined that emission from the T_2 state is unlikely.

To conclude, we have demonstrated with the example of fac-Ir(ppy)$_3$ that the methods described in this paper represent a powerful tool to study the emission properties of organic luminescent molecules. Work is now in progress to include the effect of temperature on the emission spectra.

ACKNOWLEDGMENTS

This research is supported by Solvay and the National Science Foundation (in the framework of the CRIF Program under Award No. CHE-0443564 and the STC Program under Award No. DMR-0120967).

[1] K. King, P. Spellane, and R. Watts, J. Am. Chem. Soc. **107**, 1431 (1985).
[2] F. Garces, K. Dedeian, N. Keder, and R. Watts, Acta Crystallogr., Sect. C: Cryst. Struct. Commun. **49**, 1117 (1993).
[3] F. Allen and O. Kennard, Chemical Design Automation News **8**, 31 (1993).
[4] M. Baldo, D. O'Brien, M. Thompson, and S. Forrest, Phys. Rev. B **60**, 14422 (1999).
[5] M. Baldo and S. Forrest, Phys. Rev. B **62**, 10958 (2000).
[6] P. Hay, J. Phys. Chem. A **106**, 1634 (2002).
[7] W. Finkenzeller and H. Yersin, Chem. Phys. Lett. **377**, 299 (2003).
[8] J. Breu, P. Stossel, S. Schrader, A. Starukhin, W. J. Finkenzeller, and H. Yersin, Chem. Mater. **17**, 1745 (2005).
[9] K.-C. Tang, K. Liu, and I.-C. Chen, Chem. Phys. Lett. **386**, 437 (2004).
[10] T. Tsuboi and N. Aljaroudi, IEICE Electron. Express **1**, 281 (2004).
[11] N. A. T. Tsuboi, Opt. Mater. (Amsterdam, Neth.) **27**, 1859 (2005).
[12] K. Nozaki, J. Chin. Chem. Soc. (Taipei) **53**, 101 (2006).
[13] Y. Divayana and X. Sun, Phys. Rev. Lett. **99**, 143003 (2007).
[14] E. Jansson, B. Minaev, S. Schrader, and H. Agren, Chem. Phys. **333**, 157 (2007).
[15] S. Sprouse, K. King, P. Spellane, and R. Watts, J. Am. Chem. Soc. **106**, 6647 (1984).
[16] M. Baldo, D. O'Brien, Y. You, A. Shoustikov, S. Sibley, M. Thompson, and S. Forrest, Nature (London) **395**, 151 (1998).
[17] W. Finkenzeller, P. Stoßel, and H. Yersin, Chem. Phys. Lett. **397**, 289 (2004).
[18] C. Daniel, Top. Curr. Chem. **241**, 119 (2004).
[19] J.-J. K. C.-L. Lee, and K. B. Lee, Appl. Phys. Lett. **77**, 2280 (2000).
[20] M. T. R. C. Kwong and S. Lamansky, Adv. Mater. (Weinheim, Ger.) **12**, 1134 (2000).
[21] M. Baldo, M. Thompson, and S. Forrest, Nature (London) **403**, 750 (2000).
[22] M. F. Herman and E. Kluk, Chem. Phys. **91**, 27 (1984).
[23] E. Kluk, M. Herman, and H. Davis, J. Chem. Phys. **84**, 326 (1986).
[24] M. Rini, J. Dreyer, E. T. Nibbering, and T. Elsaesser, Chem. Phys. Lett. **374**, 13 (2003).
[25] Y. Wu and V. S. Batista, J. Chem. Phys. **124**, 224305 (2006).
[26] T. E. Sharp and H. M. Rosenstock, J. Chem. Phys. **41**, 3453 (1964a).
[27] G. J. Small, J. Chem. Phys. **54**, 3300 (1971).

[28] A. M. Mebel, M. Hayashi, K. K. Liang, and S. H. Lin, J. Phys. Chem. A **103**, 10674 (1999).
[29] G. M. Sando, K. G. Spears, J. T. Hupp, and P. T. Ruhoff, J. Phys. Chem. **105**, 5317 (2001).
[30] G. M. Sando and K. G. Spears, J. Phys. Chem. **105**, 5326 (2001).
[31] T. E. Sharp and H. M. Rosenstock, J. Chem. Phys. **41**, 3453 (1964b).
[32] D. Gruner and P. Brumer, Chem. Phys. Lett. **138**, 310 (1987).
[33] P. T. Ruhoff, Chem. Phys. **186**, 355 (1994).
[34] A. Toniolo and M. Persico, J. Comput. Chem. **22**, 968 (2001).
[35] M. Hayashi, A. M. Mebel, K. K. Liang, and S. H. Lin, J. Chem. Phys. **108**, 2044 (1998).
[36] C. Manneback, Physica **17**, 1001 (1951).
[37] A. B. Myers, *Biological Application of Raman Spectroscopy* (Wiley, New York, 1987), Vol. 2.
[38] I. R. Levine, *Molecular Spectroscopy* (Wiley, New York, 1975).
[39] S. H. Lin, Theor. Chim. Acta **10**, 301 (1968).
[40] M. Born and K. Huang, *Dynamical Theory of Crystal Lattices* (Clarendon, Oxford, 1954).
[41] E. J. Heller, J. Chem. Phys. **68**, 2066 (1978).
[42] E. J. Heller, J. Chem. Phys. **68**, 3891 (1978).
[43] E. J. Heller, Acc. Chem. Res. **14**, 368 (1981).
[44] M. D. Feit, J. A. Fleck, and A. Steiger, J. Comput. Phys. **47**, 412 (1982).
[45] S. H. Lin, C. H. Chang, K. K. Liang, R. Chang, Y. J. Shiu, J. M. Zhang, T.-S. Yang, M. Hayashi, and F. C. Hsu, Adv. Chem. Phys. **121**, 1 (2002).
[46] Y. Wu and V. S. Batista, J. Chem. Phys. **118**, 6720 (2003).
[47] Y. Wu and V. S. Batista, J. Chem. Phys. **121**, 1676 (2004).
[48] D. V. Shalashilin and M. S. Child, Chem. Phys. **304**, 103 (2004).
[49] D. V. Shalashilin, M. S. Child, and D. C. Clary, J. Chem. Phys. **121**, 3563 (2004).
[50] M. D. Feit and J. A. Fleck, J. Chem. Phys. **78**, 301 (1983).
[51] D. Kosloff and R. Kosloff, J. Comput. Phys. **52**, 35 (1983).
[52] R. Kosloff, Annu. Rev. Phys. Chem. **45**, 145 (1994).
[53] N. Makri, Annu. Rev. Phys. Chem. **50**, 167 (1999), and references therein.
[54] M. H. Beck, A. Jackle, G. A. Worth, and H. D. Meyer, Phys. Rep. **324**, 1 (2000).
[55] W. H. Miller, Proc. Natl. Acad. Sci. U.S.A. **102**, 6660 (2005).
[56] M. Ben-Nun, J. Quenneville, and T. J. Martinez, J. Phys. Chem. A **104**, 5161 (2000).
[57] M. Ben-Nun and T. J. Martinez, Adv. Chem. Phys. **121**, 439 (2002).
[58] S. Y. Kim and S. Hammes-Schiffer, J. Chem. Phys. **119**, 4389 (2003).
[59] H. B. Wang and M. Thoss, J. Phys. Chem. A **107**, 2126 (2003).
[60] P. H. Nguyen and G. Stock, J. Chem. Phys. **119**, 11350 (2003).
[61] Q. Shi and E. Geva, J. Chem. Phys. **121**, 3393 (2004).
[62] A. Donoso and C. C. Martens, J. Chem. Phys. **116**, 10598 (2002).
[63] O. V. Prezhdo and Y. V. Pereverzev, J. Chem. Phys. **113**, 6557 (2000).
[64] T. D. Hone and G. A. Voth, J. Chem. Phys. **121**, 6412 (2004).
[65] S. Bonella and D. F. Coker, J. Chem. Phys. **114**, 7778 (2001).
[66] A. E. Cardenas, R. Krems, and R. D. Coalson, J. Phys. Chem. A **103**, 9469 (1999).
[67] L. Turi and P. J. Rossky, J. Chem. Phys. **120**, 3688 (2004).
[68] M. Nest and P. Saalfrank, Chem. Phys. **268**, 65 (2001).
[69] S. J. Jang and J. S. Cao, J. Chem. Phys. **114**, 9959 (2001).
[70] A. Sergi, D. MacKernan, G. Ciccotti, and R. Kapral, Theor. Chem. Acc. **110**, 49 (2003).
[71] D. E. Makarov and H. Metiu, J. Chem. Phys. **111**, 10126 (1999).
[72] S. S. Zhang and E. Pollak, J. Chem. Phys. **119**, 11058 (2003).
[73] D. Antoniou and S. D. Schwartz, J. Chem. Phys. **119**, 11329 (2003).
[74] J. L. Gao and D. G. Truhlar, Annu. Rev. Phys. Chem. **53**, 467 (2002).
[75] M. H. M. Olsson, P. E. M. Siegbahn, and A. Warshel, J. Am. Chem. Soc. **126**, 2820 (2004).
[76] I. R. Craig and D. E. Manolopoulos, J. Chem. Phys. **121**, 3368 (2004).
[77] D. Neuhauser, J. Chem. Phys. **100**, 9272 (1994).
[78] W. Zhu, J. Z. H. Zhang, and D. H. Zhang, Chem. Phys. Lett. **292**, 46 (1998).
[79] G. C. Schatz, M. S. Fitzcharles, and L. B. Harding, Faraday Discuss. **84**, 359 (1987).
[80] D. C. Clary, J. Phys. Chem. **98**, 10678 (1994).
[81] J. R. Fair, D. Schaefer, R. Kosloff, and D. J. Nesbitt, J. Chem. Phys. **116**, 1406 (2002).
[82] J. Echave and D. C. Clary, J. Chem. Phys. **100**, 402 (1994).
[83] H. G. Yu and J. T. Muckerman, J. Chem. Phys. **117**, 11139 (2002).
[84] M. I. Hernandez and D. C. Clary, J. Chem. Phys. **101**, 2779 (1994).
[85] J. M. Bowman, J. Phys. Chem. A **102**, 3006 (1998).
[86] D. Q. Xie, R. Q. Chen, and H. A. Guo, J. Chem. Phys. **112**, 5263 (2000).
[87] S. M. Anderson, T. J. Park, and D. Neuhauser, Phys. Chem. Chem. Phys. **1**, 1343 (1999).
[88] X. Chen and V. S. Batista, J. Chem. Phys. **125**, 124313 (2006).
[89] K. G. Kay, J. Chem. Phys. **100**, 4377 (1994a).
[90] K. G. Kay, Annu. Rev. Phys. Chem. **56**, 255 (2005).
[91] K. G. Kay, Chem. Phys. **322**, 3 (2006).
[92] Y. Wu and M. F. Herman, J. Chem. Phys. **125**, 154116 (2006).
[93] V. Guallar, V. S. Batista, and W. H. Miller, J. Chem. Phys. **113**, 9510 (2000).
[94] K. G. Kay, J. Chem. Phys. **100**, 4432 (1994b).
[95] R. Ahlrichs, M. Bär, H.-P. Baron, R. Bauernschmitt, S. Böcker, N. Crawford, P. Deglmann, M. Ehrig, K. Eichkorn, S. Elliott, F. Furche, F. Haase, M. Häser, H. Horn, C. Hättig, C. Huber, U. Huniar, M. Kattannek, A. Köhn, C. Kölmel, M. Kollwitz, K. May, P. Nava, C. Ochsenfeld, H. Öhm, H. Patzelt, A. Schäfer, D. Rappoport, O. Rubner, A. Schafer, U. Schneider, M. Sierka, O. Treutler, B. Unterreiner, M. von Arnim, F. Weigend, P. Weis, and H. Weiss, TURBOMOLE V5.9.1, Universität Karlsruhe, 2007.